



## Fatigue crack growth assessments in welded components including crack closure effects: Experiments and 3-D numerical modeling

Diego F.B. Sarzosa<sup>a</sup>, Leonardo B. Godefroid<sup>b</sup>, Claudio Ruggieri<sup>a,\*</sup>

<sup>a</sup> Department of Naval Architecture and Ocean Engineering, University of São Paulo, São Paulo, Brazil

<sup>b</sup> Department of Materials Science and Metallurgy, Federal University of Ouro Preto, Ouro Preto, Brazil

### ARTICLE INFO

#### Article history:

Received 3 February 2012

Received in revised form 11 September 2012

Accepted 16 September 2012

Available online 26 September 2012

#### Keywords:

Fatigue crack growth

Crack closure

Fatigue tests

Steel welds

Numerical modeling

### ABSTRACT

This work provides a numerical and experimental investigation of fatigue crack growth behavior in steel weldments including crack closure effects and their coupled interaction with weld strength mismatch. A central objective of this study is to extend previously developed frameworks for evaluation of crack closure effects on FCGR to steel weldments while, at the same time, gaining additional understanding of commonly adopted criteria for crack closure loads and their influence on fatigue life of structural welds. Very detailed non-linear finite element analyses using 3-D models of compact tension  $C(T)$  fracture specimens with center cracked, square groove welds provide the evolution of crack growth with cyclic stress intensity factor which is required for the estimation of the closure loads. Fatigue crack growth tests conducted on plane-sided, shallow-cracked  $C(T)$  specimens provide the necessary data against which crack closure effects on fatigue crack growth behavior can be assessed. Overall, the present investigation provides additional support for estimation procedures of plasticity-induced crack closure loads in fatigue analyses of structural steels and their weldments.

© 2012 Elsevier Ltd. All rights reserved.

### 1. Introduction

Accurate assessments of the fatigue life for structural components and their weldments remain essential in design, fabrication and safe operation of critical engineering structures, including pressure vessels, piping systems, offshore oil facilities, bridges and cranes among others. Typical welding processes introduce strong thermal cycles and inhomogeneous residual stresses in the weld metal and surrounding region (including the HAZ) which often deteriorate the metallurgical quality and potentially lower the fatigue life of the weldment [1]. The reduced fatigue performance of the weld joint (as compared with the base plate material) largely increases the likelihood of failure from the crack propagation of an undetected weld defect. Experimental observations consistently reveal the occurrence of a variety of crack-like defects in the welded region which are either planar (e.g., hot or cold cracking, lack of penetration, undercut) or volumetric (e.g., porosity and entrapped slag) [2,3] even if good workmanship and proper selection of the welding procedure and filler-metal composition are employed. Indeed, the history of in-service weldment failures over the past decades clearly reveal that fatigue cracking represents a major source of catastrophic fracture in fabricated steel structures [3].

Conventional fatigue design of unwelded structural components based on stress-life approaches most often employs simpli-

fied models incorporating an implicit crack initiation criterion which essentially link the nominal stress range,  $\Delta S$ , or nominal stress amplitude,  $S_a$ , with the material's fatigue strength [4]. These approaches have led to a substantial broadening of fatigue analyses of cyclic loaded structures while, at the same time, producing conservative predictions of the fatigue life for several classes of structural components. However, the much higher incidence of weld flaws, coupled with a relatively large variety of weld joint geometries, greatly complicates generalization and direct extension of conventional stress-life procedures to fatigue design of welds thereby prompting further developments in fatigue strength assessments of load-carrying welded joints. The early work of Gurney [5] introduced the concept of fatigue design curves ( $S \times N$ ) for welded steel joints in which each specific design curve reflects the general influence of weld geometry, weld details and residual stresses on the fatigue life. Within Gurney's approach, these  $S \times N$  curves range from a ground flush butt welded joint (highest fatigue strength) to a transverse fillet welded joint (lowest fatigue strength) [6]. Subsequent study by Gurney and Maddox [7] derived from a statistical analysis of experimental fatigue data provided the basis for a number of current standards and guidelines incorporating design curves representing 95% survival probability for a given weld detail or weld joint configuration such as, for example, AWS D1.1 [8], BS 7608 [9] and DNV C-203 [10] among others. A comprehensive investigation on the fatigue behavior of welded components including fatigue strength assessments and design rules is given by Maddox [11] and Lassen and Récho [12].

\* Corresponding author. Tel.: +55 11 30915184; fax: +55 11 30915717.

E-mail address: [claudio.ruggieri@poli.usp.br](mailto:claudio.ruggieri@poli.usp.br) (C. Ruggieri).

While stress-life fatigue analyses have been used effectively in many structural applications, it is now generally recognized that crack propagation from pre-existing defects dominates the fatigue life of welded joints. Consequently, advanced procedures for fatigue assessments of critical weldments should include the effects of crack extension under cyclic loading on fatigue life predictions for structural components.

Experimental studies reveal that fatigue crack growth rates (FCGR) in welds may display strong sensitivity to welding process, weld geometry, localized changes in material and mechanical properties of the weldment, including the heat affected zone. These effects arise from the complex interplay between macroscale features (crack size and geometry, material properties including weld strength mismatch, weld residual stresses, load ratio, etc.) and the micromechanism of fatigue crack growth. At the macroscale regime, there is a clear correlation between crack propagation rate under cyclic loading and load ratio ( $R$ ) in which the FCGR increases with  $R$ . Here, crack closure effects play a key role in controlling the rate of crack propagation with varying load ratios by strongly affecting the (effective) stress intensity factor (SIF) range. However, despite the technological importance of fatigue crack extension in welded structural components, a full understanding of the fatigue crack growth phenomenon in welds remains limited as does a more extensive body of experimental data. Early work of Benoit et al. [13] on fatigue crack propagation in the heat affected zone (HAZ) for a structural steel weld showed that FCGR in welded materials are lower than the corresponding rates in the base plate material. Link [14] conducted FCGR experiments using compact tension specimens for both the base plate and weldments of a 5456-H116 aluminum alloy and an ASTM A710 Grade A steel with and without post-weld heat treatment (PWHT); these results show a strong influence of welding residual stresses on the measured FCGRs due to the effects of crack closure. Later, Shankar and Wu [15] showed that fatigue crack growth behavior in welded 5083-H321 aluminum alloys is essentially similar to the parent material. These previous research efforts clearly demonstrate that accurate evaluation procedures for effective stress intensity factors which are applicable to welded fracture specimens remain essential in more refined defect assessment procedures capable of including effects of crack closure on fatigue crack growth rates.

Motivated by these observations, this work provides a numerical and experimental investigation of fatigue crack growth behavior in steel weldments including crack closure effects and their coupled interaction with weld strength mismatch. A central objective of this study is to extend previously developed frameworks for evaluation of crack closure effects on FCGR to steel weldments while, at the same time, gaining additional understanding of commonly adopted criteria for crack closure loads and their influence on fatigue life of structural welds. Very detailed non-linear finite element analyses using 3-D models of compact tension  $C(T)$  fracture specimens with center cracked, square groove welds provide the evolution of crack growth with cyclic stress intensity factor which is required for the estimation of the closure loads. Fatigue crack growth tests conducted on plane-sided, shallow-cracked  $C(T)$  specimens provide the necessary data against which crack closure effects on fatigue crack growth behavior can be assessed. Overall, the present investigation provides additional support to estimation procedures of plasticity-induced crack closure loads in fatigue analyses of structural steels and their weldments.

## 2. Brief perspective on fatigue crack growth including crack closure

Elber's pioneering work [16] on plasticity-induced crack closure (PICC) provided a major impetus for bringing new concepts and a

more comprehensive understanding to bear on problems of fatigue crack propagation. While a number of other closure mechanisms have since received considerable attention, PICC remains as the primary mechanism in stage II fatigue crack growth associated with acceleration and retardation effects under cyclic loading as well as load ratio effects and short crack behavior in fatigue among others. Much research has been continuously spent in the past years aiming at developing adequate techniques to describe PICC and its effects on fatigue crack growth behavior. This section provides a brief overview of fatigue crack growth description including crack closure effects. The presentation that follows also introduces key features of the evaluation procedures for crack closure loads more widely adopted in fatigue crack growth analysis.

### 2.1. Overview of fatigue crack growth description

In the context of small scale yielding (SSY) conditions and limited-scale plasticity, existing models generally describe crack extension under constant cyclic loading in the form [17–19]

$$\frac{da}{dN} = f(\Delta K, R) \quad (1)$$

where  $\Delta K = K_{max} - K_{min}$  is the (macroscopic) stress intensity range,  $R = K_{min}/K_{max}$  defines the load ratio and  $da/dN$  denotes the amount of crack growth per cycle. Here,  $K_{max}$  and  $K_{min}$  represent the maximum and minimum values of the elastic stress intensity factor,  $K$ . A widely adopted simplified form of previous Eq. (1) applicable to characterize the stage II of crack growth behavior in metals is given by a power law defined as

$$\frac{da}{dN} = C(\Delta K)^m \quad (2)$$

where  $C$  and  $m$  are material's constants. The above Eq. (2) is often known as Paris law [17–19].

However, even though the mechanism of fatigue crack growth associated with Eq. (2) (and, consequently, Eq. (1)) is strictly associated with SSY conditions and well-contained plasticity at the crack tip, the large tensile plastic strains that develop ahead of the growing fatigue crack tip are not fully reversed during subsequent unloading [20,21]. This results in formation of a plastic wake associated with compressive residual stresses behind the fatigue crack tip which causes crack face contact before complete unloading. This phenomenon was first observed by Elber [16] and is most often referred to as plasticity-induced crack closure (PICC).

Because of premature crack face contact due to the PICC mechanism just discussed, the stress intensity level at which Mode I opening loading,  $K_{op}$ , starts "driving" fatigue crack growth is larger than  $K_{min}$ . Elber [16] defined an effective stress intensity factor range given by  $\Delta K_{eff} = K_{max} - K_{op} = U\Delta K$  so that Eq. (2) is rewritten as

$$\frac{da}{dN} = C(\Delta K_{eff})^m = C(U\Delta K)^m \quad (3)$$

in which  $U$  defines the closure ratio given by  $U = \Delta K_{eff}/\Delta K$ .

Inclusion of closure effects in fatigue crack growth analysis reveals features that can be different from those emerging through application of the conventional treatment given by previous Eq. (2). Based on the interpretation of  $\Delta K_{eff}$  as the effective cyclic driving force for fatigue crack extension, it becomes clear the potential strong effect of PICC on crack growth rates under constant amplitude cyclic loading. Consequently, accurate estimations of crack closure stresses appear central in engineering analyses which can effectively predict fatigue crack growth from crack-like flaws and defects as will be addressed next.

## 2.2. Crack closure evaluation procedures in fatigue crack growth analysis

There is a history of research efforts aimed at developing engineering approaches to evaluate crack closure loads. Most of evaluation procedures to estimate crack closure loads in fatigue testing of common fracture specimens have evolved essentially along two lines of development: (1) indirect estimation based on experimental measurements of specimen compliance variation due to contact of crack faces and (2) numerical evaluation of crack closure loads based on finite element descriptions of fatigue crack propagation. Approaches falling in the first category may be viewed as macroscopic procedures since they rely entirely on experimental measurements of load–displacement records to relate the macroscale variation of specimen compliance with the microscale closure loads; here the measured specimen compliance,  $C_m$ , (which is the inverse of the specimen stiffness) is defined as the relationship between displacement, most often characterized in terms of crack mouth opening displacement (CMOD), and applied load in the form  $C_m^{CMOD} = V_m/P_m$ . In contrast, numerical simulations of crack propagation by fatigue enable a local evaluation of closure loads over size scales which are similar to the size of the fracture process zone associated with fatigue crack extension.

Because of its relative ease with which the load–displacement records can be measured in conventional test specimens, the indirect method is most suited for testing protocols measuring crack closure loads such as ASTM E647 [22]. However, while employed extensively to estimate crack closure loads due to its relative simplicity, analysis of the compliance variation during fatigue cycling may exhibit significant difficulties in accurate evaluations of crack flank contact based on global measurements of load with CMOD. Representative works of this technique include the methodologies proposed by Schijve [23] and Carman et al. [24]. These procedures essentially define the closure load,  $P_{cl}$ , based on an approximate description for key portions of the experimentally measured

$P$ -CMOD curve as illustrated in Fig. 1. Here, the increased tensile loading ranging from  $P_{min}$  to  $P_{max}$  depicted in this plot can be described by four distinct regions depending on the measured compliance and whether the crack faces are in contact or the crack has extended: (1) Region AB corresponds to a linear relationship between load and displacement for which the crack is fully closed; (2) Region BC marks the beginning of crack opening thereby causing a nonlinear evolution of load with CMOD with consequent increase (decrease) in specimen compliance (stiffness); (3) the crack is fully open in Region CD but no significant crack growth nor plastic deformation occur so that specimen compliance remains constant; and (4) finally, crack growth and plastic deformation take place in Region DE for which there is further increase (decrease) in specimen compliance (stiffness).

By assuming that the closure load,  $P_{cl}$ , has the same (absolute) value of the opening load,  $P_{op}$ , the general features previously observed support the viewpoint that  $P_{cl}$  (or, equivalently,  $P_{op}$ ) can be defined as the load value corresponding to the point marking the transition between region BC and CD (see Fig. 1). Because the measured  $P$ -CMOD curve is a discrete, rather than continuous, function, Schijve [23] defined the opening load,  $P_{op}$ , as the value corresponding to the intersection between a linear fitting of region CD and a quadratic fitting for region AC. While a few other evaluation schemes have been proposed (see, e.g., the review of Stoychev and Kujawsky [25]), Schijve's approach has proven effective in determining crack closure loads [26].

Despite the apparent simplicity of (macroscopic) compliance-based techniques, numerical schemes to evaluate crack closure loads based upon finite element analyses have been receiving increasingly attention. Early progress in developing numerical techniques to describe PICC was achieved by Newman [27] and McClung and Sehitoglu [28]. Approaches based on finite element simulations of fatigue crack propagation essentially rely on an adequate modeling of crack-tip behavior and the surrounding near-tip region to describe the closure mechanism. Most often, these methodologies implement widely adopted techniques in which a finite

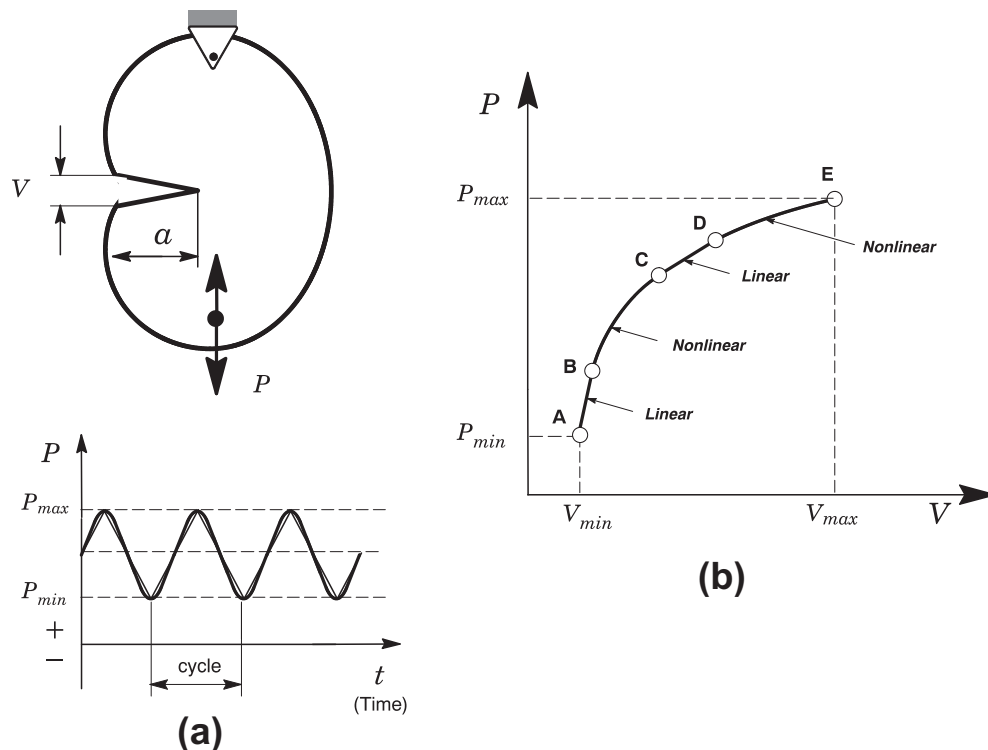


Fig. 1. Schematic illustration of closure effects on the evolution of cyclic load versus crack opening displacement for an arbitrary cracked body.

element crack model is cyclic loaded between minimum and maximum values of prescribed remote stresses. Within each load cycle, crack extension occurs through conventional nodal release thereby advancing the crack by one element size. The residual plastic deformation region which develops behind the advancing crack front enables defining the closure/opening loads and, consequently, estimates of  $K_{op}$ -values. While relatively simple, several modeling issues often complicate fatigue crack growth simulations and have a direct bearing on the computed closure/opening loads. These issues include mesh refinement, details of the node release scheme, opening load stabilization with increased crack extension, crack face contact and, perhaps more importantly, the criterion to define when the crack closes and opens.

Much work has been done on numerical modeling of PICC based on the finite element method which led to a number of criteria to define the levels of crack closure loads. Standard finite element analysis of fatigue crack propagation typically defines the opening loads based on the displacement and stress fields measured on nodes adjacent to the crack tip. The early work of Newman [27] and McClung and Sehitoglu [28] introduced a simple criterion in which  $P_{op}$  was identified as the applied remote load at which the first node behind the current crack front opens relative to the crack plane. Sehitoglu and Sun [29] and Wu and Ellyin [30] advanced this viewpoint by defining the crack opening when the near-tip opening stress, which was compressive in previous cycle, changes from compression to tension; here, they simply identified the opening load as the load level at which the opening nodal stress at the crack tip changes from negative to a positive value. More recently, Roychowdhury and Dodds [31] proposed an alternative criterion in which  $P_{op}$  was identified as the applied remote load at which the second node behind the current crack front opens relative to the crack plane.

While all previous approaches have been relatively effective in describing closure effects for fatigue assessment applications, they remain rather limited with few comparisons between numerical predictions and experimentally measured results [32–34]. Moreover, the large differences in predicted closure loads depending on the adopted criterion to define  $P_{op}$  reported in the literature [35,36] raise some concerns on the robustness of these methodologies. The analyses described subsequently address these issues and explore further extensions of crack closure criteria to describe fatigue crack growth behavior for steel weldments.

### 3. Numerical modeling of plasticity-induced crack closure

#### 3.1. Finite element description of fatigue crack growth analysis

Fig. 2a illustrates a simplified view of fatigue crack growth in elastic–plastic materials under macroscopic Mode I loading. Development of plasticity-induced crack closure is related to plastic deformation left in the wake of the growing crack by cyclic loading. Fig. 2b shows the finite element representation of the crack-tip region including the crack wake (contact region) behind the advancing crack. Within the 3-D framework adopted in the present work, constrained nodes on the crack plane (which is also the symmetry plane) define the crack ligament. Crack growth occurs by uniform release of the constrained nodes defining the current crack front thereby advancing the crack.

Numerical simulation of fatigue crack propagation is based on a sufficiently refined mesh such as the effects of forward and reversed plasticity can be adequately described within the near-tip region, including the plastic wake zone behind the crack. A single row of uniformly sized, squared elements arranged along the crack ligament enables fatigue crack extension by an amount equals to the element size,  $l_e$ , in each cycle. Competing demands dictate the choice of the element size: (1) adequate resolution of the stress–strain fields over a small, narrow region near the crack tip and (2) number of cycled which is necessary to simulate fatigue crack propagation. As described below, numerical crack propagation by fatigue occurs by nodal release so that a very large number of loading and unloading cycles (order of thousand cycles) is required if the element size,  $l_e$ , is too small. Conversely, using larger  $l_e$ -values would likely result in poor representation of the near-tip stress and strain fields as well as the plastic wake region thereby affecting estimates of crack closure loads. In previous work employing similar procedure, Roychowdhury and Dodds [31] utilized element sizes ranging from 0.005 to 0.02 mm. This range of values for  $l_e$  satisfies issue (2) while providing satisfactory resolution of the near-tip fields required in issue (1). In the present 3-D analyses, we adopt  $l_e = 0.02$  mm for the homogeneous C (T) specimens and  $l_e = 0.01$  mm for welded C (T) configuration described later. Moreover, such element sizes also enable including at least three elements within the reverse plastic zone at all crack front locations [31] for both material conditions. Preliminary numerical analyses [37] to simulate crack closure in a single edge cracked tension SE (T) specimen agree very well with the results obtained

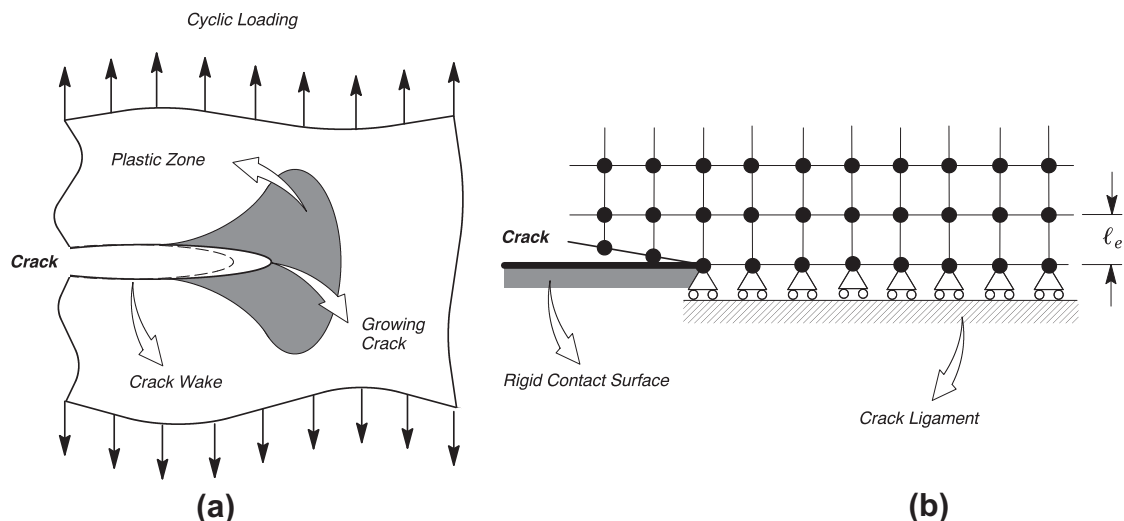


Fig. 2. Simplified model of fatigue crack growth in elastic–plastic materials under macroscopic Mode I loading.

by Daniewicz and Ismonov [35] thereby providing strong support to our adopted approach.

The remote load is applied under load control conditions by cycling it from  $P_{min}$  to  $P_{max}$  in a triangular-type wave, i.e., the load increases linearly from  $P_{min}$  to  $P_{max}$  and then decreases also linearly from  $P_{max}$  to  $P_{min}$ . The crack propagates by an amount  $\Delta a = l_e$  in each cycle by releasing the crack-tip node at the beginning of the unloading step corresponding to that cycle (see Fig. 1a). Frictionless contact over the crack flanks is enforced by using a rigid surface at the crack symmetry plane to prevent crack surface penetration as described next (see Fig. 2b).

### 3.2. Crack closure criteria

The computational framework for fatigue crack growth modeling adopted here enables defining the crack closure loads based on  $K_{op}$ -values using essentially three different methodologies: (a) node displacement procedure, (b) crack-tip stress evolution and (c) specimen compliance measurements. Fig. 3 illustrates the essential features of crack opening evaluation using the first two methodologies for a growing crack in the  $xy$ -plane; fatigue crack growth occurs along the  $x$ -axis in which unconstrained (released) nodes define the crack face with its origin at the current crack tip. For the node displacement procedure, a widely adopted approach utilizes the concept of node contact to the (rigid) crack plane to characterize the opening load. Here,  $P_{op}$  is defined when the vertical displacement of the first node,  $V_y^{fn}$ , behind the crack tip becomes positive during the opening phase of the loading cycle. Alternatively,  $P_{op}$  can also be defined based on the same strategy but using the vertical displacement of the second node,  $V_y^{sn}$ , behind the crack tip. In contrast, the second methodology utilizes the crack-tip node to assess crack opening but evaluates changes in crack-tip opening stresses rather than vertical displacements. Here,  $P_{op}$  is defined when the crack-tip opening stress (which corresponds to the crack-tip nodal stress,  $\sigma_{yy}^{ctn}$ ) changes from compression to tension during the opening phase of the loading cycle.

A number of previous studies have used the first two procedures (either directly or in slightly modified forms) to model crack closure loads in common fracture specimens against which experimentally measured closure loads are compared. McClung and Davidson [33] analyzed middle-crack tension  $M(T)$  specimens with short cracks ( $a/W \approx 0.1 \sim 0.3$ ) made of a 7091 aluminum alloy. By using similar numerical techniques developed in previous work of McClung and Sehitoglu [28], they found good agreement between experimentally measurements and numerical predictions of near-tip strains, crack opening displacements and crack closure loads. Wei and James [38] conducted a study of fatigue crack closure in polycarbonate compact tension  $C(T)$  specimens and showed that closure loads measured using the specimen compliance technique are within 10–15% of the numerical predictions based on the

first-node displacement criterion. More recently, Simandjuntak et al. [32] and Kim et al. [39] performed 3-D finite element analyses coupled with the first-node displacement criterion to predict closure loads in middle-crack tension  $M(T)$  specimens made of 2024 and 7075 aluminum alloys which are in good agreement with experiments.

The third methodology to evaluate crack closure loads based upon specimen compliance follows entirely the procedure using the compliance offset method described in ASTM E647 [22] standard. Here,  $P_{op}$  is determined from tracing the changes in specimen compliance due to closure of the crack derived from the computed evolution of load vs. displacement with increasing crack advance for the analyzed numerical models. When the crack becomes fully open during the loading portion of the load cycle, the specimen compliance attains a characteristic value,  $\tilde{C}_m$ , and remains essentially unchanged upon further loading until large scale yielding conditions prevail in the crack-tip region. Upon unloading from the peak load attained in a cycle, the specimen compliance still has the characteristic value,  $\tilde{C}_m$ , for the fully-open crack. Consequently, the  $P_{op}$ -value corresponds to the force at which the measured load vs. displacement in a cycle becomes linear (point C in previous Fig. 1). While conceptually simple, a fully open load is difficult to identify during the evolution of load vs. displacement due to the gradual and rather subtle change in specimen compliance as it approaches the open-crack value. By defining the opening load as the load corresponding to a compliance that is offset from the fully-open-crack value rather than the load at which the compliance attains the fully-open value (the point at which the curve becomes linear), evaluation of the  $P_{op}$ -value within each cycle becomes less sensitivity to the inherent noise and nonlinearity in the measurement system [22]. The selection of an appropriate compliance offset criterion remains somewhat arbitrary although it is clear that its choice should ideally reduce the scatter and errors in  $P_{op}$ -estimates. Readers are referred to ASTM E647 [22] for additional details.

### 3.3. 3-D finite element models

3-D finite element analyses are conducted on a plane sided 0.5-T C (T) specimen ( $B = 12.5$  mm) with  $W = 50$  mm and having a square groove weld with a fixed weld groove width,  $2h$ . The analysis matrix includes C (T) specimens having varying crack size to specimen width ratio:  $a/W = 0.2, 0.25, 0.30, 0.35, 0.4, 0.5, \text{ and } 0.6$ . Here,  $a$  is the crack length,  $W$  is the specimen width and  $B$  is the specimen thickness. The geometry and material flow properties match those for specimens tested in the experiments described in Section 4 (see Fig. 6a).

Fig. 4a shows the finite element model constructed for the 3-D analyses of the C (T) specimen previously described having  $a/W = 0.6$ . Symmetry conditions enable analyses using one-quarter, 3-D model of the specimen. This 3-D model has

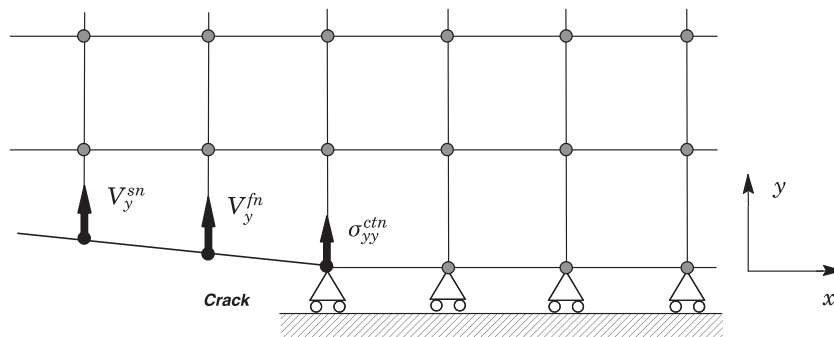


Fig. 3. Crack opening criteria adopted in the present work to define the opening load,  $P_{op}$ .

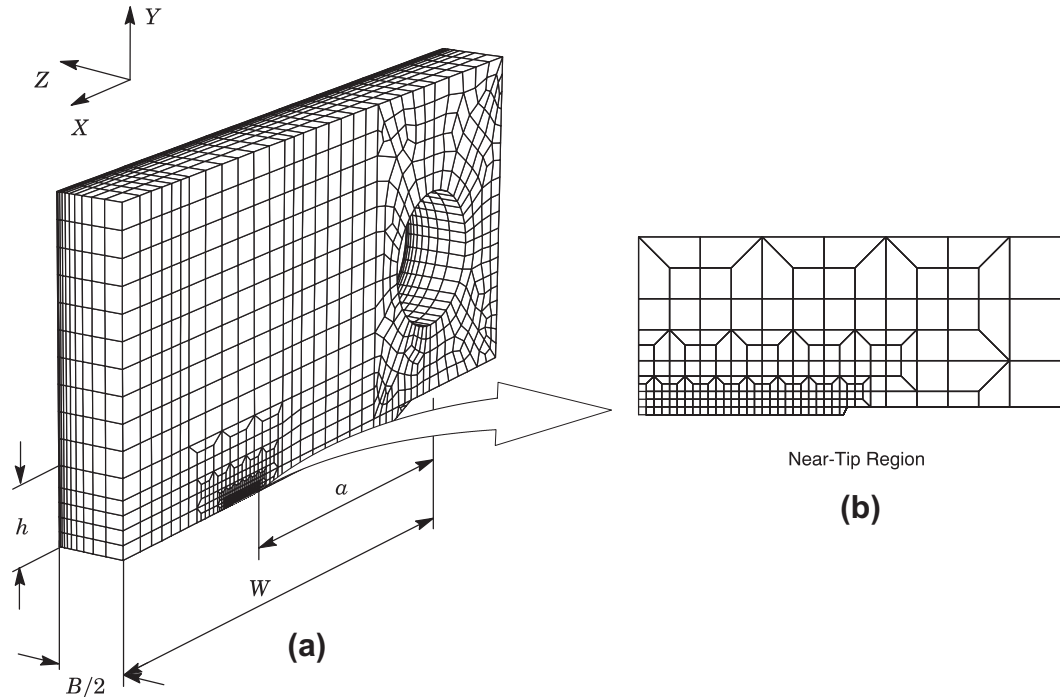


Fig. 4. (a) Finite element model constructed for the 3-D analyses of the C(T) specimen having  $a/W = 0.6$  and (b) near-tip region with squared cells along the remaining ligament.

approximately 10100 8-node elements ( $\sim 13,200$  nodes) arranged into 10 variable thickness layers over the half-thickness ( $B/2$ ), as illustrated in Fig. 4a. This refinement in the thickness direction proved highly effective to resolve the out-of-plane ( $Z$ -direction) stresses. Within each of the 10 layers over the crack front, the element mesh contains a row of 200 squared cells along the remaining ligament ( $W - a$ ) arranged as shown in Fig. 4b. A series of numerical experiments suggest an optimal cell size of  $l_e = 20 \mu\text{m}$  for the homogeneous specimen and  $l_e = 10 \mu\text{m}$  for the welded specimen so that the slab of 2000 ( $10 \times 200$ ) squared cells over which fatigue crack growth occurs can extend up to 2–4 mm uniformly over the half-thickness ahead of the initial crack front. Fatigue crack propagation takes place under load control conditions in which the prescribed forces are imposed at the pin hole indicated in Fig. 4a.

#### 3.4. Material models and finite element procedures

Evaluation of plasticity-induced crack closure loads requires nonlinear finite element solutions which include the effects of the plastic wake behind the crack tip on crack face contact. These analyses utilize an incremental, isotropic hardening constitutive model to describe the cyclic, elastic–plastic response of the material in small geometry change (SGC) setting. The numerical solutions employ a simple power-hardening model to characterize the uniaxial true stress ( $\bar{\sigma}$ )-logarithmic strain ( $\epsilon$ ) in the form

$$\frac{\epsilon}{\epsilon_{ys}} = \frac{\bar{\sigma}}{\sigma_{ys}} \quad \epsilon \leq \epsilon_{ys}; \quad \frac{\epsilon}{\epsilon_{ys}} = \left( \frac{\bar{\sigma}}{\sigma_{ys}} \right)^n \quad \epsilon > \epsilon_{ys} \quad (4)$$

where  $\sigma_{ys}$  and  $\epsilon_{ys}$  are the yield stress and strain, and  $n$  is the strain hardening exponent.

The finite element analyses consider material flow properties for an ASTM A516 Grade 70 and its weldment. Section 4 provides the tensile and mechanical properties for the analyzed materials and describes the uniaxial true stress vs. logarithm strain curves for the ASTM A516 steel (base plate and overmatch weld material) at

the test temperature,  $T = 20 \text{ }^\circ\text{C}$ ; these curves were used in the finite element computations reported here. To facilitate addressing effects of weld strength mismatch on fatigue crack growth, it proves convenient to define the mismatch ratio,  $M_y$ , as

$$M_y = \frac{\sigma_{ys}^{WM}}{\sigma_{ys}^{BM}} \quad (5)$$

where  $\sigma_{ys}^{BM}$  and  $\sigma_{ys}^{WM}$  denote the yield stress for the base metal and weld metal.

The finite element code WARP3D [40] provides the numerical solutions for the 3-D analyses reported here. The code enables conventional linear elastic analysis and incorporates both a Mises ( $J_2$ ) constitutive model in both small-strain and finite-strain framework. To simulate the contact interaction between the closing crack face to the rigid crack plane (see Fig. 2b), WARP3D implements frictionless, rigid-body contact using a simple penalty method to enforce displacement constraints in the solution of the finite element model by creating springs at the contact points. The spring stiffness corresponds to the penalty parameter, while the amount of remaining penetration corresponds to the error in the enforcement of the constraint. WARP3D adds each spring stiffness into the corresponding element stiffness matrices instead of directly into the global stiffness matrix.

## 4. Experimental program

### 4.1. Tested materials and fatigue specimens

The material utilized in this study was a normalized pressure vessel steel ASTM A516 Gr 70 with 16 mm thick base plate. A multipass butt weldment using the shielded metal arc welding (SMAW) process was produced with an overmatch between the yield strength of the base plate material and weld metal. A single-V type groove was used for fabrication of the test weld through an adequate choice of weld filler material and welding parameters. Fig. 5a provides a schematic of the weld joint profile along with a summary of the geometry and welding variables for the weldment.

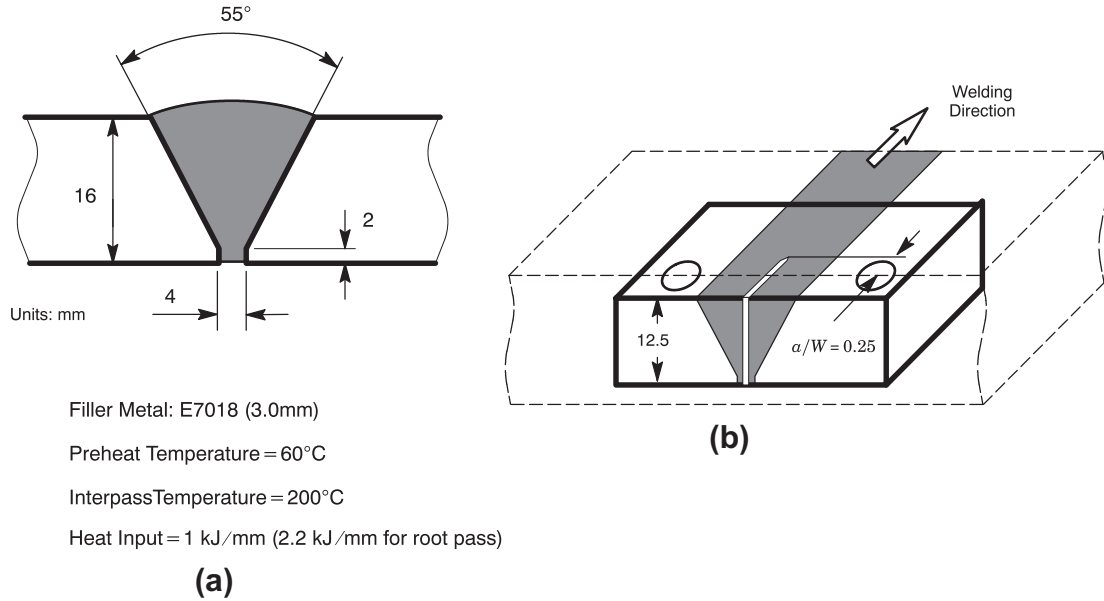


Fig. 5. (a) Schematic of the weld joint profile from which the fatigue specimens were extracted and (b) compact C(T) specimen used in fatigue testing.

Mechanical tensile tests, conducted on longitudinal tensile specimens (ASTM E8), provide the room temperature (20 °C) stress–strain data for the base plate and weld materials. The test specimens for the weldments were machined from the weld fusion zone with their longitudinal axes parallel to the welding direction. Fig. 6a shows the true stress–logarithmic strain curves for the base plate and weldments. Table 1 summarizes the tensile data for the tested materials (average of three tensile tests) and indicates that the weldment overmatches the base plate material by 45% ( $M_y = 1.45$  – refer to Eq. (5) for definition of the mismatch level) at room temperature.

4.2. Experimental fatigue crack growth data

Fatigue crack growth tests at room temperature (20 °C) were conducted on plane-sided C(T) specimens with a fixed crack length to width ratios,  $a/W = 0.25$ , illustrated in Fig. 5b. The specimens have width,  $W = 50.8$  mm, thickness  $B = 12.5$  mm, and were extracted in the T–L orientation for the base plate material and in the longitudinal weld direction for the weld material. The test matrix includes two C(T) specimens for the base plate material and two C(T) specimens for the weld material. The fatigue crack growth experiments were performed on a servo-hydraulic testing machine

Table 1

Mechanical properties of tested ASTM A516 Gr70 steel at room temperature.

Material	$\sigma_{ys}$ (MPa)	$\sigma_u$ (MPa)	$\sigma_u/\sigma_{ys}$
Base plate	351	526	1.50
Weld metal	511	580	1.14

$\sigma_{ys}$ : 0.2% proof stress;  $\sigma_u$ : ultimate tensile strength.

at a frequency of 30 Hz (sine wave) under load control and constant amplitude loading with load ratio,  $R = 0.1$ . The current crack length in the specimens was estimated based upon a compliance procedure using the cyclic evolution of load vs. crack mouth opening displacement (CMOD) records as previously outlined.

Post-weld heat treatment (PWHT) at 590 °C for 30 min with controlled, slow cooling was performed on the welded specimens to promote stress relief in the weld joint. Evaluation of the residual stresses on the specimen surface was made using an X-ray diffraction technique. X-ray diffraction uses the distance between crystallographic planes as a strain gage measurement (see, for example, Anderoglu [41], for additional details). The residual deformation produces changes in the spacing of lattice plane from their stress free value to a new value that corresponds to the magnitude of

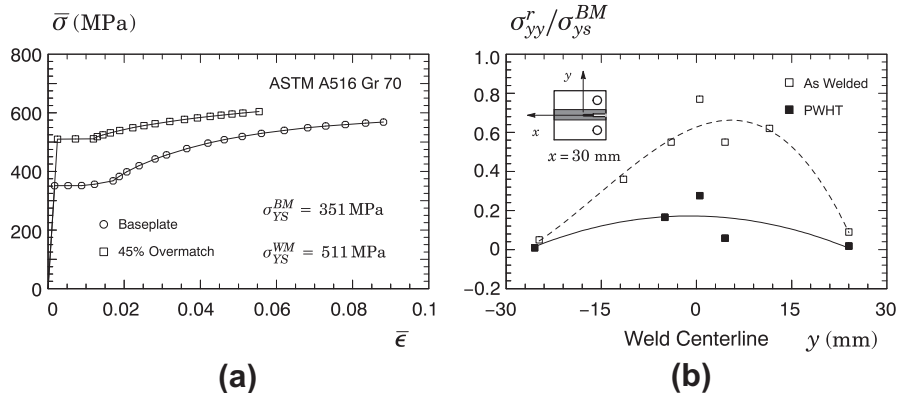


Fig. 6. (a) True stress–logarithmic strain curves for the baseplate and weldments and (b) distribution of residual stress across the weld centerline,  $\sigma_{yy}^r$ , normalized by the yield stress for the base plate material,  $\sigma_{BM}^{ys}$ , measured at  $x = 30$  mm.

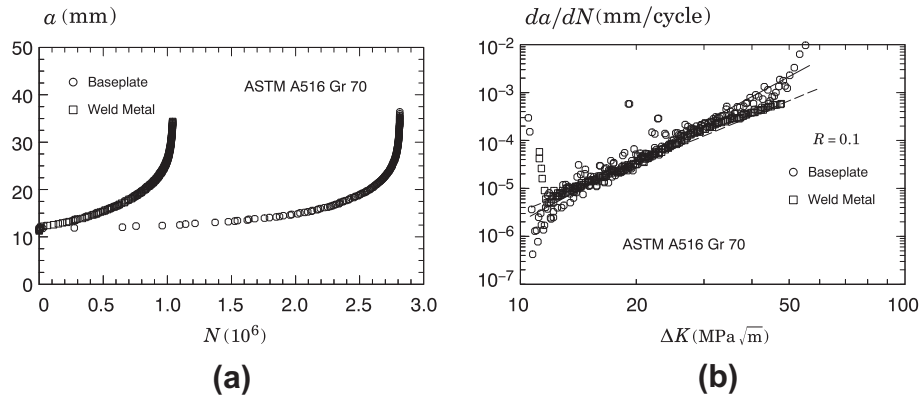


Fig. 7. Experimentally measured fatigue crack growth data for the C(T) specimens with both test conditions: (a) base plate material and (b) 45% overmatch weld.

**Table 2**  
Coefficients C and m defining the linear fitting on the log-log plot corresponding to the Paris law describing the experimental data in stage II region.

Data set	Linear fitting	
	m	C (Mpa, m)
Base plate	3.85	$4.46 \times 10^{-10}$
45% Overmatch weld	3.38	$1.92 \times 10^{-9}$

the residual stress. The diffraction measurements were carried out on a Shimadzu XRD-7000 diffractometer. The average of four incidence angles, ( $0^\circ$ ,  $5^\circ$ ,  $30^\circ$ , and  $40^\circ$ ), was utilized to calculate the residual stress values. Fig. 6b provides the measured distribution of residual stresses normal to crack plane,  $\sigma_{yy}^r$ , normalized by  $\sigma_{ys}^{BM}$ , with the distance from the center of seam weld before and after the PWHT. In this plot, the open and solid symbols correspond to the measured residual stress values whereas the lines represent a cubic fit to the experimental points. The residual stress values,  $\sigma_{yy}^r$ , were measured at a remote distance from the crack tip,  $x=30$  mm. While the applied PWHT does not fully eliminate the weld residual stress fields, it reduces significantly the residual stress levels; here, the  $\sigma_{yy}^r$ -values do not exceed  $\sim 25\%$  of the base plate's yield stress.

Fig. 7a and b displays the experimentally measured fatigue crack growth data for the C(T) specimens with both test conditions: base plate material and 45% overmatch weld. Two different levels of maximum load were imposed during the tests:  $P_{max} = 720$  kgf e  $P_{max} = 900$  kgf. As expected, the fatigue crack growth rate is not influenced by the level of maximum applied load. Thus, only the results for the maximum load level corresponding to  $P_{max} = 720$  kgf are presented here. The straight lines included in Fig. 7b

represent the linear fitting on the log-log plot corresponding to the Paris law (refer to previous Eq. (2)) describing the experimental data in stage II region. Table 2 provides the coefficients C and m for both data sets. Here, while the slope of both curves are similar, the coefficient C which characterizes the rate of crack propagation is more strongly affected by the overmatch condition.

### 5. Crack closure effects on fatigue behavior

#### 5.1. Thickness effects on closure loads

Before undertaking the 3-D crack closure analyses of the C(T) specimens, it is instructive to first examine the variation of the closure loads over the specimen thickness for the homogeneous C(T) specimen. Fig. 8a and b shows the computed crack closure loads,  $P_{op}$ , normalized by  $P_{max}$  with the amount of crack growth,  $\Delta a$ , normalized by the initial size of crack-tip plastic zone, denoted as  $\bar{r}_p$ , at five different locations over the specimen half-thickness for the crack configuration with  $a/W = 0.35$ ,  $z/B = 0, 0.217, 0.347, 0.487$ , and  $0.5$  for two different closure criteria: (i) 1st-node displacement and (ii) 2nd-node displacement. Here,  $z$  is the Cartesian axes perpendicular to the crack plane (see Fig. 4) and  $B$  is the specimen thickness so that  $z/B = 0$  corresponds to the specimen center-plane and  $z/B = 0.5$  defines the specimen surface. Further,  $\bar{r}_p$  is simply taken as Irwin's approximation for the size of crack-tip plastic zone [17] defined by  $\bar{r}_p = (K_I^0 / \sigma_{ys})^2 / (3\pi)$  in which  $\sigma_{ys}$  is the material's yield stress and  $K_I^0$  represents the Mode I stress intensity factor determined for the initial crack size,  $a_0$ . In these plots,  $P_{max}$  is taken the value of 720 kgf.

The trends displayed in these plots are clear. Closure effects are maximum at the specimen surface ( $z/B = 0.5$ ) when the closure

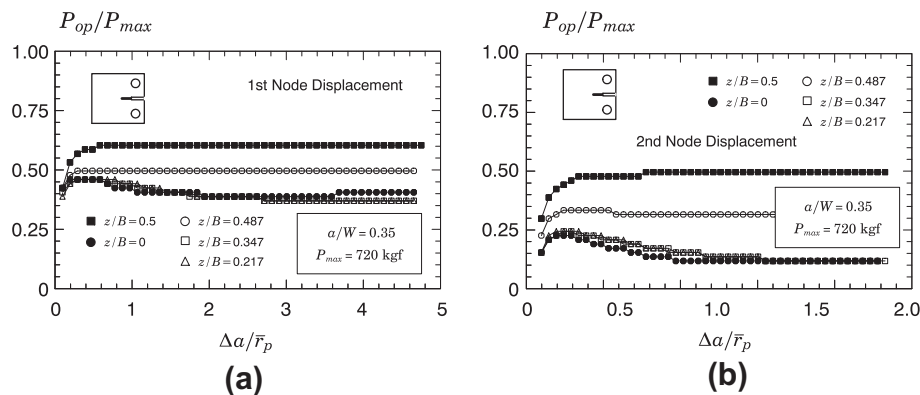


Fig. 8. Computed normalized crack closure loads,  $P_{op}$ , with the amount of normalized crack growth,  $\Delta a$ , at five different crack-front locations and varying crack closure criteria.



loads reach a peak value (relative to the load level  $P_{max}$ ) and then fall very rapidly after a short distance from the surface. Consider, for example, the evolution of the normalized  $P_{op}$  with normalized  $\Delta a$  derived from using the 1st-node displacement criterion provided in Fig. 8a. The closure load has a peak value of  $P_{op}/P_{max} \approx 0.6$  and drops to  $P_{op}/P_{max} \approx 0.38$  at  $z/B \leq 0.347$ ; similar behavior is observed for the results shown in Fig. 8b derived from using the 2nd-node displacement criterion (note, however, that the  $P_{op}/P_{max}$ -values are consistently lower for all five crack front locations,  $z/B$ ). Similar results are obtained for other crack configurations with different  $a/W$ -ratios; to conserve space, they are not shown here.

This behavior can be understood in terms of the plastic wake development at the near-tip region which remains relatively small for most of the specimen inner region but increases substantially when the specimen surface is approached. Therefore, the fully developed plastic zone formed in front of the growing crack tip at the specimen surface brings about an increase in the closure loads which most likely controls the overall fatigue crack advance. These observations support the viewpoint of evaluating the closure loads at specimen surface as addressed next.

5.2. 3-D crack closure analyses for C(T) specimens

The extensive 3-D finite element analyses of the C(T) specimen configurations provide the evolution of crack-tip displacements and stresses to define the closure loads in terms of the criteria previously described. Figs. 9–11 display the key results relating the variation of  $P_{op}$  with cyclic crack extension in the analyzed fatigue specimens. The material properties for the analyses covered in these plots correspond to the ASTM A516 Gr 70 for the base plate and 45% overmatch conditions.

Figs. 9 and 10 shows the evolution of  $P_{op}$  normalized by  $P_{max}$  with the amount of crack growth,  $\Delta a$ , normalized by the initial size of crack-tip plastic zone, denoted as  $\bar{r}_p$ , for two widely different crack sizes, as defined by the  $a/W$ -ratio. As already discussed in previous section, these  $P_{op}$ -values correspond to the closure loads evaluated at the crack front location defined at  $z/B = 0.5$ . The present study focuses on numerical simulations corresponding to  $P_{max} = 720$  kgf; Sarzosa [42] also describes additional analyses with other levels of maximum load and found trends qualitatively similar to the results shown in Figs. 9 and 10. In these plots, the  $P_{op}$ -values attain a “plateau” following a short transient at early stages of loading associated with development of near-tip plasticity. Analogous features are also observed for other  $a/W$ -ratios; these results are not shown here in interest of space.

A strong effect of the adopted closure criterion on  $P_{op}$ -values can be seen in Figs. 9 and 10. Further, observe that the  $P_{op}$ -values are also affected, albeit to a lesser degree, by increased crack sizes. Consider first the deep crack results shown in Figs. 9b and 10b. The 1st-node displacement criterion consistently produces the highest closure loads for both the base plate and overmatch condition whereas the specimen compliance criterion results in the lowest closure loads. Consider now the shallow crack results shown in Figs. 9a and 10a. The 1st-node displacement criterion also produces the highest closure load for the base plate condition. In contrast, however, the specimen compliance criterion now results in the highest closure load for the overmatch condition. We also draw attention to a comparison among the local criteria covering the 1st-node and 2nd-node displacement as well as the crack-tip stress criterion. For all analyzed cases, the 2nd-node displacement criterion always gives the lowest closure loads irrespective of crack size and whether base plate or overmatch condition is considered.

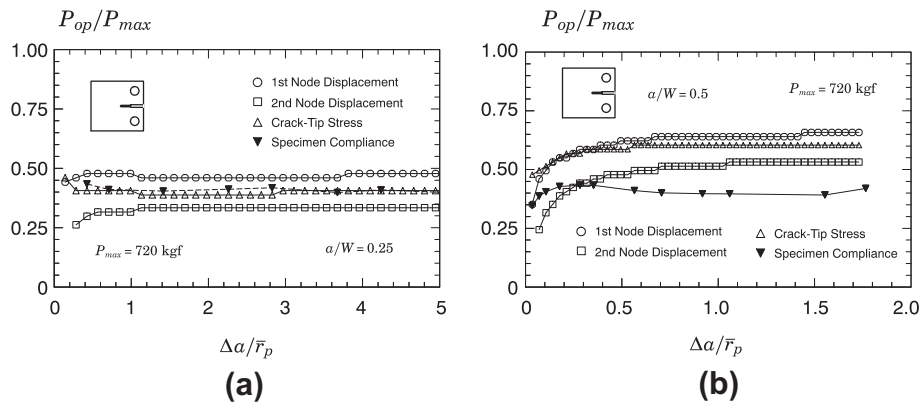


Fig. 9. Evolution of  $P_{op}$  normalized by  $P_{max}$  with the amount of crack growth,  $\Delta a$ , normalized by  $\bar{r}_p$ , for the base plate C (T) specimen with different  $a/W$ -ratios.

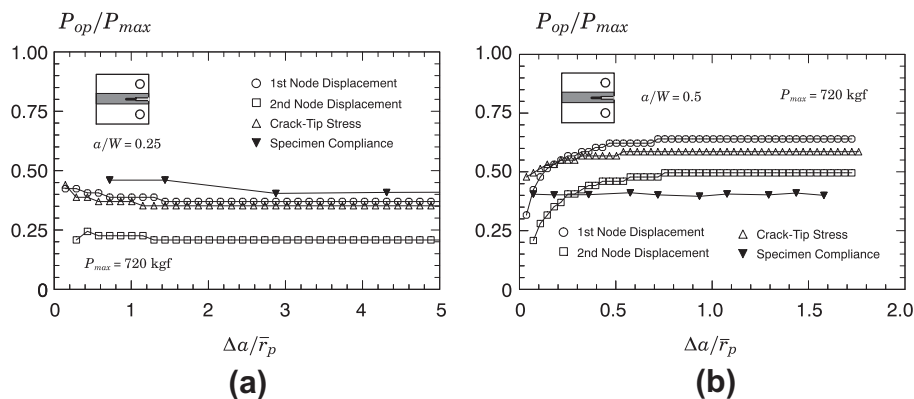


Fig. 10. Evolution of  $P_{op}$  normalized by  $P_{max}$  with the amount of crack growth,  $\Delta a$ , normalized by  $r_p$ , for the overmatched weld C(T) specimen with different  $a/W$ -ratios.

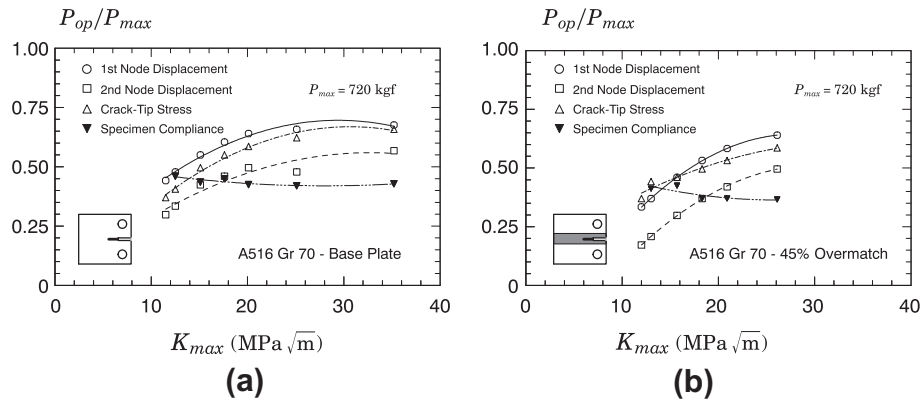


Fig. 11. Evolution of the normalized closure load,  $P_{op}/P_{max}$ , with increased values of  $K_{max}$ , for both base plate and overmatch condition.

Now, using the results displayed in previous Figs. 9 and 10 with the inclusion of corresponding results for other  $a/W$ -ratios, Fig. 11 shows the evolution of the normalized closure load,  $P_{op}/P_{max}$ , with increased values of  $K_{max}$ , for both base plate and overmatch condition. Here, since the applied maximum load is kept constant during the analyses, i.e.,  $P_{max} = 720$  kgf, the  $K_{max}$ -value is directly associated with each analyzed  $a/W$ -ratio. Further, the  $P_{op}$ -value for each analyzed crack configuration is taken as the “plateau” value attained in the analyses. The significant features include: (1)  $P_{op}$ -values increase with increased values of  $K_{max}$  for all local criteria and both material conditions (base plate and overmatch weld); (2)  $P_{op}$ -values decrease with increased values of  $K_{max}$  for the specimen compliance criterion; (3)  $P_{op}$ -values are generally higher for the base plate material when compared to corresponding values for the overmatch weld; and (4) the 1st-node displacement criterion produces the highest closure loads with increased values of  $K_{max}$  for both material conditions.

5.3. Fatigue behavior including closure effects

To examine the influence of crack closure loads as determined by the previous evaluation criteria, Figs. 12 and 13 shows the fatigue crack growth response for the  $C(T)$  specimens in logarithmic scale with both material conditions (base plate material and 45% overmatch weld) corrected for closure effects. Here,  $\Delta K_{eff} = K_{max} - K_{op}$  as previously defined. To facilitate comparison, these plots also include the experimental fatigue crack growth data measured using the tested  $C(T)$  specimens presented previously in Section 4.2. Since they represent the experimentally measured data (no closure effects are considered), the corresponding fatigue curves are expressed in terms of  $\Delta K$  rather than  $\Delta K_{eff}$  as indicated in the plots.

The sets of results in Figs. 12 and 13 demonstrate that fatigue crack growth response for the tested materials can be strongly affected by the adopted crack closure criterion. From these results, some key conclusions can be drawn. First, the 1st-node

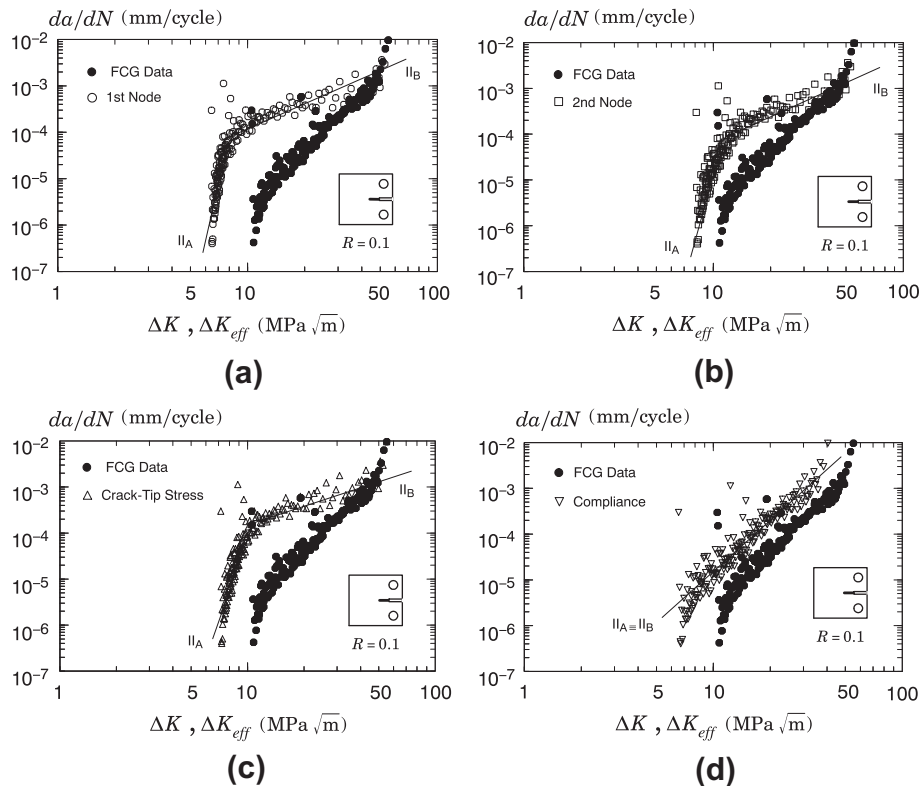


Fig. 12. Fatigue crack growth response for the  $C(T)$  specimens with base plate material corrected for closure effects using different crack closure criteria.

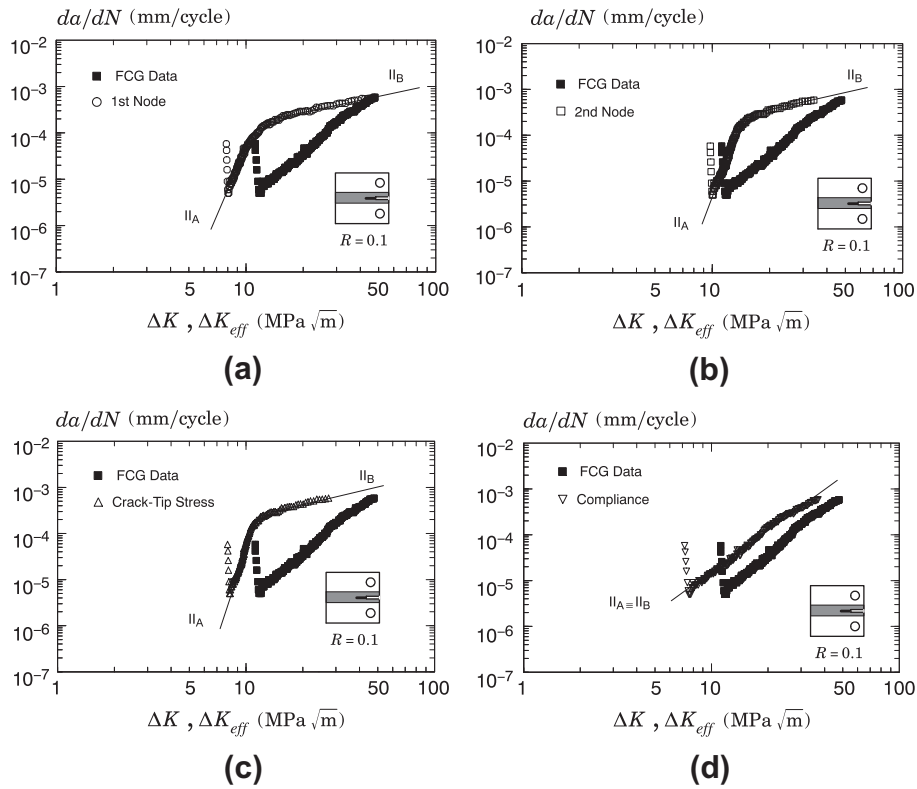


Fig. 13. Fatigue crack growth response for the C(T) specimens with overmatch weld corrected for closure effects using different crack closure criteria.

displacement criterion yields the largest correction of the measured fatigue curves. Second, the effects of crack closure on the measured fatigue curves are more prominent at early stages of fatigue crack growth corresponding to lower values of applied  $\Delta K$ , particularly for the 1st and 2nd node displacement criteria. At later stages of fatigue crack extension (higher  $\Delta K$ -values), however, closure effects on the fatigue curves appear to diminish. Third, the relative effects of crack closure on the measured fatigue curves are similar irrespective of whether the base plate or overmatch material are considered.

#### 5.4. Crack closure effects on fatigue life predictions

To further demonstrate the effects of crack closure criteria on fatigue behavior, the previously corrected curves are used to predict the fatigue life of the tested C(T) specimens for both material conditions. The evolution of  $da/dN$  with  $\Delta K_{eff}$  for all sets of results displayed in Figs. 12 and 13 provides the basis to determine the number of cycles to failure,  $N_f$ , based on integration of the modified Paris law described by previous Eq. (3). Such an analysis serves as a prototype for a wide class of integrity assessment and remaining life problems involving fitness-for-service evaluations of structural components containing crack-like flaws such as BS 7910 [43] and API 579 [44].

However, estimation of  $N_f$  by integration of the fatigue curves corrected for closure using Eq. (3) raises practical difficulties related to the nonlinear dependence of  $\log(da/dN)$  vs.  $\log(\Delta K_{eff})$  in the region corresponding to stage II of fatigue crack propagation. As can be seen in the plots of Figs. 12 and 13, there is a clear departure of the corrected fatigue curves from a linear behavior, particularly for the 1st-node and 2nd-node displacement criteria for both material conditions. As a simple approximation, we can model such behavior by describing the evolution of  $\log(da/dN)$  vs.  $\log(\Delta K_{eff})$  as a bilinear function so that region II of fatigue crack propagation can be identified as two substages, denoted  $II_A$  and  $II_B$ .

Each substage refers to a linear dependence of  $\log(da/dN)$  vs.  $\log(\Delta K_{eff})$  thereby permitting simpler integration of Eq. (3) over substages  $II_A$  and  $II_B$ . Such a procedure is a direct analog of the methodology adopted by BS 7910 [43] and API 579 [44] to describe experimentally measured fatigue curves used in remaining life assessments.

Figs. 12 and 13 include straight lines derived from a best fit that defines the bilinear behavior of the fatigue curves corrected for closure based on the above procedure. The fit was made over the stress intensity factor range starting at  $\Delta K_{eff} = (10^{-5}/C)^{1/m}$  to the  $\Delta K_{eff}$  corresponding to final failure for the tested C (T) specimens (base plate and overmatch weld condition). Table 3 provides the coefficients C and m for each of the substages  $II_A$  and  $II_B$  corresponding to the corrected data sets which then entail integration of Eq. (3) to generate the number of cycles to failure,  $N_f$ , for each analyzed case. Table 4 compares the predicted values of  $N_f$ , denoted  $N_{f-pred}$ , and measured experimental number of cycles to failure,  $N_{f-exp}$ , for the tested C (T) specimens based upon different crack closure criteria. To facilitate interpretation of closure effects (and associated crack closure criterion) on predicted number of cycles to failure, this table also includes predicted values of  $N_f$  derived from integrating the experimentally measured fatigue curves (which are not corrected for closure).

The results displayed by these analyses are rather conclusive and reveal a clear sensitivity of fatigue life predictions on crack closure load estimates. Consider first the values of  $N_{f-pred}$  corresponding to the experimentally measured fatigue curves (for which no closure effect is included); here, the analyses largely underestimates the measured number of cycles to failure,  $N_{f-exp}$ . Now direct attention to the fatigue life predictions using the four crack closure criteria. Errors in predicted values of  $N_f$  range from  $\sim 12\%$  to less than 1% depending on the closure criterion and material condition. Overall, the significant features associated with these results

**Table 3**  
Coefficients  $C$  and  $m$  defining the bilinear fitting on the log–log plot corresponding to the Paris law describing the corrected data in substages II<sub>A</sub> and II<sub>B</sub> region.

Data set	Closure criterion	Bilinear fitting			
		Stage II <sub>A</sub>		Stage II <sub>B</sub>	
		$m$	$C$ (MPa, m)	$m$	$C$ (MPa, m)
Base plate	1st-Node displ.	16.64	$8.32 \times 10^{-20}$	1.37	$6.81 \times 10^{-6}$
	2nd-Node displ.	9.25	$1.05 \times 10^{-14}$	1.62	$2.36 \times 10^{-6}$
	Crack-tip stress	12.21	$8.40 \times 10^{-17}$	1.58	$3.99 \times 10^{-6}$
	Compliance	3.71	$3.17 \times 10^{-9}$	3.71	$3.17 \times 10^{-9}$
Overmatch weld	1st-Node displ.	7.90	$4.98 \times 10^{-13}$	0.95	$1.63 \times 10^{-5}$
	2nd-Node displ.	10.98	$4.66 \times 10^{-17}$	1.38	$5.16 \times 10^{-6}$
	Crack-tip stress	12.28	$2.93 \times 10^{-17}$	1.22	$1.11 \times 10^{-5}$
	Compliance	3.06	$1.27 \times 10^{-8}$	3.06	$1.27 \times 10^{-8}$

**Table 4**  
Comparisons of crack closure effects on predicted fatigue life for tested  $C(T)$  specimens with homogeneous material and overmatch weld.

Data set	Closure criterion	$N_{f-pred}$	$N_{f-pred}/N_{f-exp}$
Base plate ( $N_{f-exp} = 690,045$ )	No closure	555,046	0.804
	1st-Node displ.	694,924	1.007
	2nd-Node displ.	659,876	0.956
	Crack-tip stress	648,066	0.939
	Compliance	606,104	0.878
Overmatch weld ( $N_{f-exp} = 615,171$ )	No closure	508,222	0.826
	1st-Node displ.	601,653	0.978
	2nd-Node displ.	593,090	0.964
	Crack-tip stress	551,323	0.896
	Compliance	583,903	0.949

include: (1) Analyses using the 1st-node displacement criterion provide predictions of fatigue life in good agreement with the measured number of cycles to failure, yielding values of  $N_{f-pred}$  within 2% of  $N_{f-exp}$ ; however, the analyses result in nonconservative predictions for the  $C(T)$  specimen made of the base plate material; (2) there is no clear trend that could suggest a coupling between the closure criteria and material condition for the analyzed cases; for example, the specimen compliance criterion provides the largest error in fatigue life prediction for the base plate material whereas the crack-tip stress criterion translates into a lower value of  $N_{f-pred}$  for the overmatch weld; and (3) analyses using the 2nd-node displacement criterion appear to produce more consistent predictions of fatigue life since relative values of  $N_{f-pred}/N_{f-exp}$  are fairly similar irrespective of material condition.

## 6. Concluding remarks

The 3-D finite element simulations under constant amplitude loading of fatigue crack propagation provide quantitative estimates of plasticity-induced crack closure (PICC) loads for homogeneous and welded  $C(T)$  fracture specimens. The numerical computations are conducted on crack models subjected to cyclic loading under prescribed remote stresses to simulate the formation of a plastic wake behind the fatigue crack tip as the macroscopic crack advances through nodal release by one element size each cycle. Estimation of crack closure loads based on  $K_{op}$ -values derive from three different methodologies which include: (a) node displacement procedure, (b) crack-tip stress evolution and (c) specimen compliance measurements.

The extensive finite element analyses described here demonstrate a rather strong dependence of PICC load estimates on the adopted technique. For the analyzed materials and crack configurations, the 1st-node displacement criterion and, to a lesser degree, the crack-tip stress criterion provide consistently the largest estimates of PICC loads for essentially all reported cases. In contrast, the 2nd-node displacement criterion and the specimen compliance criterion produce lower estimates of PICC load; however, these two criteria

result in mixed trends as their relative differences is rather sensitive to material condition (base plate vs. overmatch weld) and crack size.

Verification analyses to compare the effectiveness of such methodologies in predicting fatigue life for structural components utilized experimentally measured fatigue crack growth data derived from plane-sided  $C(T)$  specimens made of an ASTM A516 Gr 70 steel with two mechanical and metallurgical conditions: base plate material and 45% overmatch weld. Generally good agreement is observed between predicted and experimentally measured fatigue life, particularly when a node displacement procedure is employed to estimate PICC loads. While rather limited, our exploratory analyses favor an approach based on the 2nd-node displacement criterion as it appears to provide more consistent predictions of fatigue life for the tested  $C(T)$  specimens irrespective of material condition. However, we do recognize that there are inherent uncertainties associated with key modeling and analysis issues which complicate fatigue crack growth simulations and PICC load estimates. This feature can adversely affect fatigue life predictions and potentially hinder the “correct” safety margin in remaining life assessments involving fitness-for-service evaluations of structural components containing crack-like flaws. Such observations may suggest the crack-tip stress criterion as a more appropriate approach to achieve a better balance between reasonable accuracy in PICC load estimates and adequate safety margins. Although additional experimental and numerical studies appear necessary to establish a more definite methodology for fatigue life predictions including crack closure effects applicable to structural components with varying geometry and material properties (including overmatch welds), the results presented here provide additional support for estimation procedures of plasticity-induced crack closure loads in fatigue analyses of structural steels and their weldments.

## Acknowledgement

This investigation is supported by Fundação de Amparo à Pesquisa do Estado de São Paulo (FAPESP) through a graduate scholarship (2008/54130–4) provided to the first author (DFBS).

The work of CR is supported by the Brazilian Council for Scientific and Technological Development (CNPq) through Grants 304132/2009–8 and 476581/2009–5. The authors acknowledge the useful discussions and the experimental support for the fatigue testing and residual stress measurements provided by Gustavo H.B. Donato (FEI University).

## References

- [1] Kerr WH. A review of factors affecting toughness in welded steels. *Int J Pres Ves Pip* 1976;4:119–41.
- [2] American Welding Society, *Welding handbook: welding technology*, 8th ed., vol. 1. Miami: American Welding Society; 1987.
- [3] Jutla T. Fatigue and fracture control of weldments. In: *Metals handbook. Fatigue and fracture*, Vol. 19. American Society for Metals; 1996. p. 434–49.
- [4] Dowling NE. *Mechanical behavior of materials: engineering methods for deformation, fracture and fatigue*. 2nd ed. New Jersey: Prentice Hall; 1999.
- [5] Gurney TR. *Fatigue of welded structures*. 2nd ed. Cambridge University Press; 1979.
- [6] Mayer H, Stark HL, Ambrose S. Review of fatigue design procedures for pressure vessels. *Int J Pres Ves Pip* 2000;77:775–81.
- [7] Gurney TR, Maddox SJ. A re-analysis of fatigue data for welded joints in steel. *Weld Res Int* 1973;3:1–54.
- [8] American Welding Society, *Structural welding code – steel*, AWS D1.1/D1.1M:2004; 2004.
- [9] British Institution, *Fatigue design of offshore steel structures*, BS 7608; 1993.
- [10] Det Norske Veritas, *Fatigue design of offshore steel structures*, Recommended, Practice RP-C203; 2005.
- [11] Maddox SJ. *Fatigue strength of welded structures*. 3rd ed. Boca Raton, FL: CRC Press; 2007.
- [12] Lassen T, Récho N. *Fatigue life analyses of welded structures*. London: ISTE Ltd; 2006.
- [13] Benoit D, Lieurade H-P, Truchon M. A study of the propagation of fatigue cracks in the heat-affected zones of welded joints in E-36 steel. In: *European Offshore Steels Research Seminar*, Cambridge, United Kingdom; 1978.
- [14] Link LR. Fatigue crack growth of weldments. In: McHenry HI, Potter JM, editors. *Fatigue and fracture testing of weldments*. ASTM STP, 1058. Philadelphia: American Society for Testing and Materials; 1990. p. 16–33.
- [15] Shankar K, Wu W. Effect of welding and weld repair on crack propagation behavior in aluminum alloy 5083 plates. *Mater Des* 2002;23:201–8.
- [16] Elber W. Fatigue crack closure under cyclic tension. *Eng Fract Mech* 1970;5:37–45.
- [17] Anderson TL. *Fracture Mechanics: Fundamentals and Applications*. 3rd ed. Boca Raton, FL: CRC Press; 2005.
- [18] Suresh S. *Fatigue of Materials*. 2nd ed. Cambridge: Cambridge University Press; 1998.
- [19] Stephens RI, Fatemi A, Stephens RR, Fuchs HO. *Metal fatigue in engineering*. New York: John Wiley & Sons; 2001.
- [20] Solanki K, Daniewicz SR, Newman JC. Finite element analysis of plasticity-induced fatigue crack closure: An overview. *Eng Fract Mech* 2004;71:149–71.
- [21] Schijve J. Four lectures on fatigue crack growth, Tech. Rep. LR-254, Delft University of Technology, Delft, The Netherlands; 1977.
- [22] American Society for Testing and Materials. Standard test method for measurement of fatigue crack growth rates, ASTM E647–08; 2008.
- [23] Schijve J. Regression analysis to find the transition from linear to non-linear function, Doc. B2–91-06 (Applications to Results of Crack Growth Measurements), Faculty of Aerospace Engineering, Delft University of Technology, The Netherlands; 1991.
- [24] Carman C, Turner C, Hillberry B. A method for determining crack opening load from load-displacement data. In: Newman JC, Elber W, editors. *Mechanics of fatigue crack growth*. ASTM STP, vol. 982. Philadelphia: American Society for Testing and Materials; 1988. p. 214–21.
- [25] Stoychev S, Kujawsky D. Method for crack opening load and crack tip shielding determination: a review. *Fatigue Fract Eng Mater Struct* 2003;26:1053–67.
- [26] Xu Y, Gregson PJ, Sinclair I. Systematic assessment and validation of compliance-based crack closure measurements in fatigue. *Mater Sci Eng A* 2000;284:114–25.
- [27] Newman JC. A finite element analysis of crack closure. In: Rice JR, Paris PC, editors. *Mechanics of Fatigue Crack Closure*. ASTM STP, vol. 590. Philadelphia: American Society for Testing and Materials; 1976. p. 281–301.
- [28] McClung R, Sehitoglu H. On the finite element analysis of fatigue crack closure – I: Basic modeling issues. *Eng Fract Mech* 1989;33:237–52.
- [29] Sehitoglu H, Sun W. Modelling of plane strain fatigue crack closure. *ASME J Eng Mater Technol* 1991;113:131–41.
- [30] Wu J, Ellyin F. A study of fatigue crack closure by elastic-plastic finite element analysis for constant-amplitude loading. *Int J Fract* 1996;82:43–65.
- [31] Roychowdhury S, Dodds RH. A numerical investigation of 3-D small-scale yielding fatigue crack growth. *Eng Fract Mech* 2003;70:2363–83.
- [32] Simandjuntak S, Alizadeh H, Smith DJ, Pavier MJ. Fatigue crack closure of a corner crack: a comparison of experimental results with finite element predictions. *Int J Fatigue* 2005;27:914–9.
- [33] McClung R, Davidson D. High resolution numerical and experimental studies of fatigue cracks. *Eng Fract Mech* 1991;39:113–30.
- [34] Matos P, Nowell D. Experimental and numerical investigation of thickness effects in plasticity-induced fatigue crack closure. *Int J Fatigue* 2009;31:1795–804.
- [35] Daniewicz S, Ismonov S. Simulation and comparison of several crack closure assessment methodologies. *Int J Fatigue* 2010;32:428–33.
- [36] Lugo M, Daniewicz S, Newman JC. A mechanics based study of crack closure measurements techniques under constant amplitude loading. *Int J Fatigue* 2011;33:186–93.
- [37] Sarzosa DFB, Ruggieri C, Godefroid LB, Donato GHB. Fatigue life estimation of welded joints including the effects of crack closure phenomena. In: 30th International Conference on Ocean, Offshore and Arctic Engineering (OMAE). Rotterdam The Netherlands; 2011.
- [38] Wei L-W, James MN. A study of fatigue crack closure in polycarbonate ct specimens. *Eng Fract Mech* 2000;66:223–42.
- [39] Kim J-S, Kang JY, Song J-H. Elucidation of fatigue crack closure behavior in surface crack by 3-d finite element analysis. *Int J Fatigue* 2007;29:168–80.
- [40] Gullerud A, Koppenhoefer K, Roy A, RoyChowdhury S, Walters M, Bichon B, et al. WARP3D: Dynamic nonlinear fracture analysis of solids using a parallel computers and workstations. *Structural Research Series (SRS 607)* UILU-ENG-95-2012, University of Illinois at Urbana-Champaign; 2004.
- [41] Anderoglu O. Residual stress measurements using x-ray diffraction, M.Sc. Thesis, Texas A&M University; 2004.
- [42] Sarzosa DFB. Fatigue life evaluation of homogeneous materials and welded joints including crack closure effects, Ph.D Thesis, University of Sao Paulo, (in Portuguese); 2012.
- [43] British Institution, *Guide to methods for assessing the acceptability of flaws in metallic structures*, BS 7910; 2005.
- [44] American Petroleum Institute, *Fitness-for-service*, API RP-579-1/ASME FFS-1; 2007.